J Appl Electrochem (2009) 39:283–291
DOI 10.1007/s10800-008-9670-8

ORIGINAL PAPER

Effects of SiC and Al_2O_3 particles on the electrodeposition of Zn, Co and ZnCo. I. Electrodeposition in the absence of SiC and Al_2O_3

Paulo C. Tulio · Ivani A. Carlos

Received: 14 February 2008 / Accepted: 19 September 2008 / Published online: 5 October 2008

Abstract Electrodeposition of Zn, Co and ZnCo from acid sulfate solutions onto steel was investigated in this first part of a study of the effects of SiC or Al_2O_3 particles on these processes and the formation of ZnCo–SiC and ZnCo–Al_2O_3 electrocomposites. Zn electrodeposition shows a well-defined pre-bulk region, where the hydrogen evolution reaction (HER) and Zn underpotential deposition (upd) compete. Zn bulk electrodeposition begins with primary nucleation and diffusion-controlled growth, strongly dependent on conditions favoring previous Zn upd against HER. It is assumed that this first bulk process takes place over the upd Zn. Zn bulk electrodeposition is followed by secondary nucleation and growth. Co electrodeposition begins with a slow $Co^{2+}_{(aq)}$ reduction in parallel with HER, followed by a faster $Co^{2+}_{(aq)}$ reduction. $Zn^{2+}_{(aq)}$ strongly hinders the initial $Co^{2+}_{(aq)}$ reduction. The ZnCo and Zn electrodeposition curves are initially similar, retaining features of pre-bulk and bulk Zn electrodeposition.

Keywords Zn, Co and ZnCo · Electrodeposition · Acid solution · Steel substrate · Electrocomposites

1 Introduction

In the last few years, there has been mounting interest in the field of electrocomposite coatings (ECC), metal-matrix composite coatings obtained by electrodeposition [1, 2]. Metal-matrix composites consist basically of a ductile metal matrix in which a second insoluble phase is dispersed [3]. For example, the dispersed particles may be hard (carbides, oxides, etc.) or lubricants (PTFE, graphite, etc.) [2]. They can vary from nanometric to micrometric sizes and can enhance significantly many properties of the deposits, including their mechanical [3–6], tribological [5, 7, 8] and anti-corrosion behavior [9, 10]. These effects depend on the content, size and type of particles being incorporated into the metal matrix [3, 5, 7, 8]. Research on ECC concentrates mainly on the influence of the incorporated particles on the properties of the composites and on the particle co-deposition mechanisms. The latter are not entirely understood [2, 11–16].

Regarding the influence of added particles on the electrodeposition curves, it has been found, in some cases, that particles suspended in the electrodeposition solution promote higher current densities [17–20]. In other cases, polarization of the electrodeposition process is observed [5, 19, 21, 22]. Webb and Robertson [22] studied Ni-γ-Al_2O_3 co-deposition and estimated that 90% of the electroactive area of the electrode would have to be blocked by particles to explain an observed polarization of 80 mV. They concluded that more complex surface blockage/adsorption effects must be present. Polarization and even depolarization caused by particles can thus be considered little understood phenomena in composite electrodeposition.

Zinc is one of the main coatings employed in the corrosion protection of steel, acting as a barrier layer or sacrificial coating [23]. Zn electrodeposition can be performed in alkaline or acid baths [24]. Current research on acid baths is mainly devoted to the effects of organic additives on Zn electrodeposition [25–32]. Alloying of Zn with small quantities of Co increases its corrosion resistance [33]. ZnCo electrodeposition is known to be anomalous, in that the less noble element, Zn, is deposited

P. C. Tulio (✉) · I. A. Carlos
Department of Chemistry, Federal University of São Carlos, Rodovia Washington Luis km 235, P.O. Box 676, CEP 13565-905 Sao Carlos, SP, Brazil
e-mail: pctulio@yahoo.com.br

in preference to the nobler one, Co. Several hypotheses have been proposed to account for anomalous electrodeposition [34–44]. In some cases, suspended ceramic particles are known to interfere with anomalous electrodeposition [5, 45, 46].

In order to achieve a good understanding of the effects of suspended particles on the electrochemistry of metal electrodeposition, it is first necessary to have a detailed characterization of the equivalent electrodeposition from particle-free solutions. The main aim of the present series of papers is the investigation of the effects of SiC and Al_2O_3 particles on the electrodepositions of Zn, Co and ZnCo and how they influence the formation of ZnCo–SiC and ZnCo–Al_2O_3 electrocomposites. In this first part, the objective is to characterize the Zn, Co and ZnCo electrodeposition processes in particle-free conditions to allow, in Part II, an evaluation of the effects of SiC and Al_2O_3 on these processes.

2 Experimental

The normal ZnCo electrodeposition solution employed was: 0.4 M $ZnSO_4 \cdot 7H_2O$ + 0.4 M $CoSO_4 \cdot 7H_2O$ + 0.3 M H_3BO_3 + 1 M NH_4Cl. A blank solution (0.3 M H_3BO_3 + 1 M NH_4Cl) and Zn (0.4 M $ZnSO_4 \cdot 7H_2O$ + 0.3 M H_3BO_3 + 1 M NH_4Cl) and Co (0.4 M $CoSO_4 \cdot 7H_2O$ + 0.3 M H_3BO_3 + 1 M NH_4Cl) electrodeposition solutions were also employed. The pH of each solution was adjusted to 2 with H_2SO_4 and all the measurements were made at this pH unless otherwise stated. All the reagents were of analytical grade and the water was distilled deionized water (ddw). The electrochemical cell was a cylindrical beaker with 150 cm^3 capacity. The working electrode (WE) was a rotating disk electrode (RDE) consisting of an interchangeable mild steel cylinder embedded in an epoxy resin, giving an electroactive flat disk surface area of 0.38 cm^2. Before each experiment WE was polished with 600-emery paper, rinsed with ddw and dried. The counter-electrode was a Pt plate (1 cm^2) and the reference electrode to which all the potentials were referred was a normal calomel electrode (NCE, 1 N KCl). The measurements were conducted at room temperature (25 °C) and current density (i)–potential (E) curves were obtained at a constant sweep rate (v) of 10 mV s^{-1}.

All electrochemical measurements were made with an Oxford Rotating Disk Electrode system. The rotation frequency (ω) was calibrated with a Strobodyn TR-5501 stroboscope. All experiments were conducted with an EG&G Instruments Model 362 Scanning Potentiostat/Galvanostat. The data were recorded in a Nicolet 310 storage oscilloscope.

Energy-dispersive X-ray spectroscopy (EDX) semi-quantitative microanalysis of ZnCo deposit surfaces was performed with a Zeiss Digital Scanning Microscope DSM-960 and an Isis Oxford Instruments Si(Li) Link EDX detector, Serial Number 21869. The films analyzed by EDX were deposited at constant galvanostatic cathodic current densities (i_g), until the deposited charge density (q_d) was 80 C cm^{-2}. By Faraday's law, this corresponds to approximately 33 μm of coating thickness, assuming 100% current efficiency.

3 Results and discussion

3.1 The electrodeposition of Zn

3.1.1 The pre-bulk electrodeposition region

Figure 1 shows typical i–E curves for the steel disk electrode in the Zn electrodeposition solution under stationary and rotating electrode conditions. These i–E profiles are very close to those for acid chloride electrodeposition solutions [47]. An expanded view of the first part of the i–E curves in Fig. 1 is provided in Fig. 2, where i–E curves for steel in the blank solution (0.3 M H_3BO_3 + 1 M NH_4Cl) are also shown. Starting from −0.6 V, under all the conditions, there is an increase in current density related to the hydrogen evolution reaction (HER): $2H_3O^+_{(aq)} + 2e^- \rightarrow H_{2(g)} + 2H_2O$. The HER, which is mass-transfer controlled (Fig. 3), exhibits smaller current densities when H_3BO_3 is in solution and H_3BO_3 also depolarizes water reduction ($2H_2O + 2e^- \rightarrow H_{2(g)} + 2OH^-_{(aq)}$). These results are in agreement with those of Zech and Landolt [48].

Figure 2 shows that HER from H_3O^+ reduction is strongly hindered with Zn^{2+} ions in solution, giving rise to

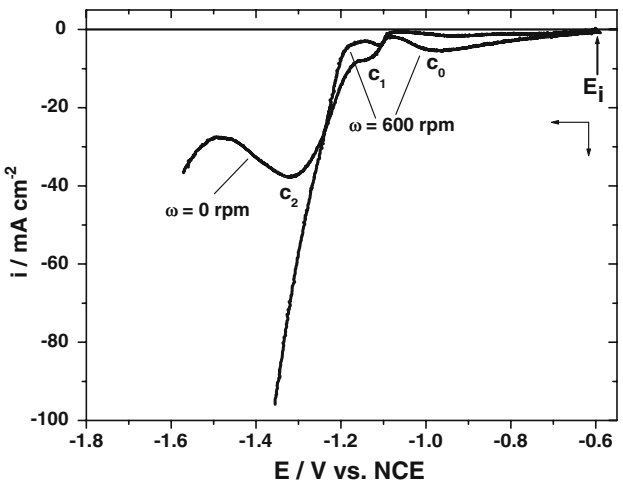

Fig. 1 Typical i–E curves for Zn electrodeposition from 0.4 M $ZnSO_4 \cdot 7H_2O$ + 0.3 M H_3BO_3 + 1 M NH_4Cl. Stationary (ω = 0 rpm) and rotating electrode conditions (ω = 600 rpm), as indicated. v = 10 mV s^{-1}. E_i: starting potential

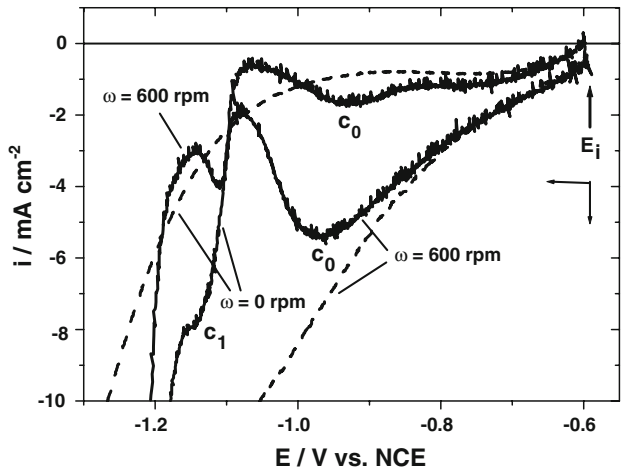

Fig. 2 Continuous lines: an expanded view of the initial part of *i–E* curves in Fig. 1. Dashed lines: *i–E* curves for the steel disk electrode in the blank solution (0.3 M H_3BO_3 + 1 M NH_4Cl). Stationary ($\omega = 0$ rpm) and rotating electrode conditions ($\omega = 600$ rpm), as indicated. $v = 10$ mV s^{-1}. E_i: starting potential

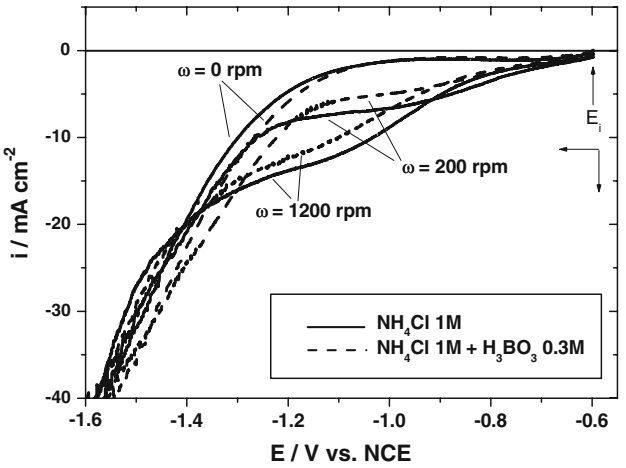

Fig. 3 Typical *i–E* curves for the steel electrode in 1 M NH_4Cl and in 1 M NH_4Cl + 0.3 M H_3BO_3 solutions at several different ω, as indicated. In all cases, $v = 10$ mV s^{-1}. E_i: starting potential

a cathodic peak c_0. With the stationary electrode, the HER is low and its contribution to the c_0 peak may be considered negligible, compared to the rotating electrode. The peak c_0 occurs in a pre-bulk deposition region since the Nernst reversible potential for the $Zn^{2+}_{(aq)}/Zn$ couple for 0.4 M of Zn^{2+} is estimated to be −1.05 V at 25 °C. This behavior is normal for Zn electrodeposition from acid solutions [25–27, 30, 49–55] and has many interpretations. It can be attributed to Zn underpotential deposition (upd) [34, 49] and Zn upd together with HER [25, 27, 30, 50–52]. Some authors, such as Lee et al. [31], consider that in this region nucleation of Zn competes with the HER. Others suggest that zinc hydroxide is formed on steel in this region, owing to the high H_3O^+ consumption [26, 53, 55]. The formation of zinc hydroxide or some dehydration product, such as ZnO, it is hard to imagine here, since there would need to be a strong alkalization at the electrode surface to reach a pH of 5.1 at which insoluble $Zn(OH)_2$ precipitates [35]. Fabri Miranda et al. [36] did not observe a sufficient rise in pH for $Zn(OH)_2$ precipitation at the beginning of ZnNi electrodeposition at pH 1.5 or 3. Baugh [56, 57] did not find reduction of ZnO films on Zn at pH 3.8 and also showed that Cl^- and NH_4^+ have a destabilizing effect on films predominantly composed of ZnO on Zn.

The steel electrode can form an iron oxide film during pre-treatment and/or even during immersion in the solution before polarization. This iron oxide film could be reduced in the cathodic scan, contributing to peak c_0. In the present study, it is assumed that no reduction of an iron oxide film occurs in this region since, in Fig. 3, there is no peak related to such a reduction or it is too small to be significant.

Hence, peak c_0 in Fig. 2 has contributions from Zn upd together with the HER from H_3O^+ reduction. The latter proceeds at a fast rate under rotating electrode conditions. The Zn upd hinders the HER by the well-known high polarization of HER on Zn substrates. As H_3O^+ competes with Zn^{2+} at active sites for adsorption [30, 31, 58, 59], a smaller area of steel is expected to be covered by Zn upd under forced convection conditions. These pre-bulk electrodeposition processes, as will be seen later, affect the bulk electrodeposition.

3.1.2 *The bulk electrodeposition*

In Figs. 1 and 2, at potentials more negative than approximately −1.06 V, the bulk electrodeposition of Zn starts. There is a first process, labeled c_1, which has an atypical behavior when stationary and rotating electrode conditions are compared. After a zone of similar current densities in both curves, with electrode rotation, the current rises to a maximum, giving rise to a peak or, sometimes, a plateau, whereas in stationary conditions, c_1 is characterized by a shoulder, reaching higher current densities than under rotating conditions. Under both conditions, after c_1, the current begins to rise again. As the scan proceeds, a mass-transfer controlled peak c_2 appears for the stationary electrode (Fig. 1). After this, the current density starts to increase again, due to the HER on Zn, together with Zn growth.

As one of the objectives of this work is to evaluate the effects of SiC and Al_2O_3 on the electrodeposition of Zn, the region c_1 and its atypical behavior with respect to ω must be understood. The influence of H_3BO_3 on process c_1 was investigated and it was demonstrated that it has effects only on the HER before peak c_0, as shown in Fig. 3.

In Fig. 4, a well-defined anodic peak can be observed when the potential sweep is reversed at a switching

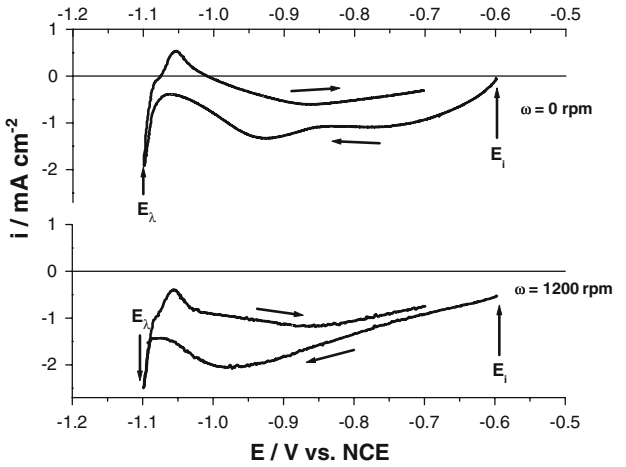

Fig. 4 Typical *i–E* curves for stationary ($\omega = 0$ rpm) and rotating electrode conditions ($\omega = 1200$ rpm), as indicated, for the zinc electrodeposition, when the potential sweep is reversed at a switching potential (E_λ) inside the region c_1. E_i: starting potential

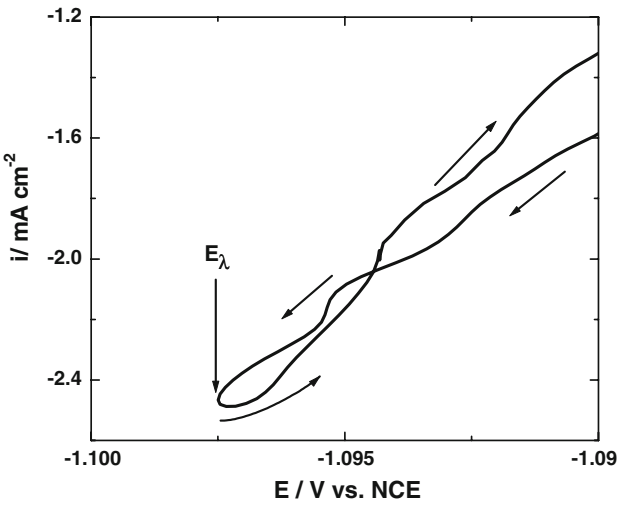

Fig. 5 Expanded view of the *i–E* behavior for zinc electrodeposition around the switching potential (E_λ) inside the region c_1, where the potential sweep is reversed. The arrows indicate the direction of potential sweep. Stationary steel electrode. $v = 10$ mV s^{-1}

potential (E_λ) inside region c_1 for the stationary electrode, indicating Zn electrodeposition. In rotating conditions, the HER is so large that it makes the total current density in the anodic scan negative, prevailing over the Zn dissolution current. Owing to the large polarization of HER on Zn, the results of Fig. 4 for rotating electrode conditions show that in c_1, the surface coverage by Zn is small, allowing the HER to occur on the steel surface. Rashkov et al. [60] observed small islands of Zn deposit on Al at the beginning of Zn electrodeposition. Also, as HER is strongly dependent on ω, H_2 bubbles may be adsorbed at the steel surface, contributing to the small coverage by Zn, as pointed out by Gomes and da Silva Pereira [26]. The same probably occurs for $\omega = 0$, but to a much lesser degree, with a higher surface coverage by Zn.

Under stationary electrode conditions, in a magnified view, a cathodic peak in the anodic scan after sweep reversal at E_λ in region c_1 is observed in Fig. 5. This characterizes nucleation and growth phenomena in the bulk region c_1.

An interesting feature of the current densities at c_1 and c_0 is that they are practically independent of [Zn^{2+}] under stationary conditions, as shown in Fig. 6a. As expected, peak c_2 is much higher at higher [Zn^{2+}] (Fig. 6b). The independence of the pre-bulk electrodeposition peak c_0 from [Zn^{2+}] may indicate a maximum adsorbed quantity of Zn [51]. The lack of dependence of both c_0 and c_1 on [Zn^{2+}] under stationary conditions shows that the same quantity of Zn is deposited and there is the same degree of coverage of steel by the Zn upd layer at both [Zn^{2+}]; also c_1 is a bulk process strictly dependent on the initial Zn upd layer. In total agreement with this interpretation are the results for the rotating electrode conditions in Fig. 6c. The fall in the current density of peak c_0 as [Zn^{2+}] increases is due to a heavier Zn upd deposited layer, which suppresses the contribution of HER. On the same basis, the current densities in c_1 are higher for 0.9 M of Zn^{2+}, showing again that the bulk c_1 region is strictly dependent on the quantity of previously deposited Zn upd.

It must be emphasized that all these processes at the beginning of Zn electrodeposition were also observed at pH = 5 and in solutions in which NH_4Cl was replaced by Na_2SO_4 in the electrolytes. With pH = 5, the atypical behavior of region c_1 with respect to ω is still present but to a lesser degree than at pH = 2, as would be expected, since the HER will be slower at this pH, leading to a higher coverage by Zn upd in the pre-bulk electrodeposition region.

Some typical voltammetric curves for the steel electrode in the Zn electrodeposition solution, now with a switching potential (E_λ) of −1.19 V, are shown in Fig. 7. It is observed that the bulk process c_1 on a rotating electrode, is under diffusion control as the current rises with ω. Moreover, there is a cathodic peak at the start of the reverse scans, showing that the new increase in current density after c_1 is related to a new nucleation and growth process. In the anodic branch of Fig. 7, a peak related to Zn electrodissolution is observed and after that, especially under rotating conditions, the current density becomes cathodic, due to the HER on the steel electrode in the same sense as in Fig. 4.

In Fig. 7 there is a significant difference in the dissolution peak areas between stationary and rotating electrode conditions. This is investigated in more detail in Fig. 8, where the anodic (q_a) to cathodic (q_c) charge density ratios ($|q_a/q_c|$) for similar experiments are displayed. The q_c values were obtained from the beginning of the bulk process c_1,

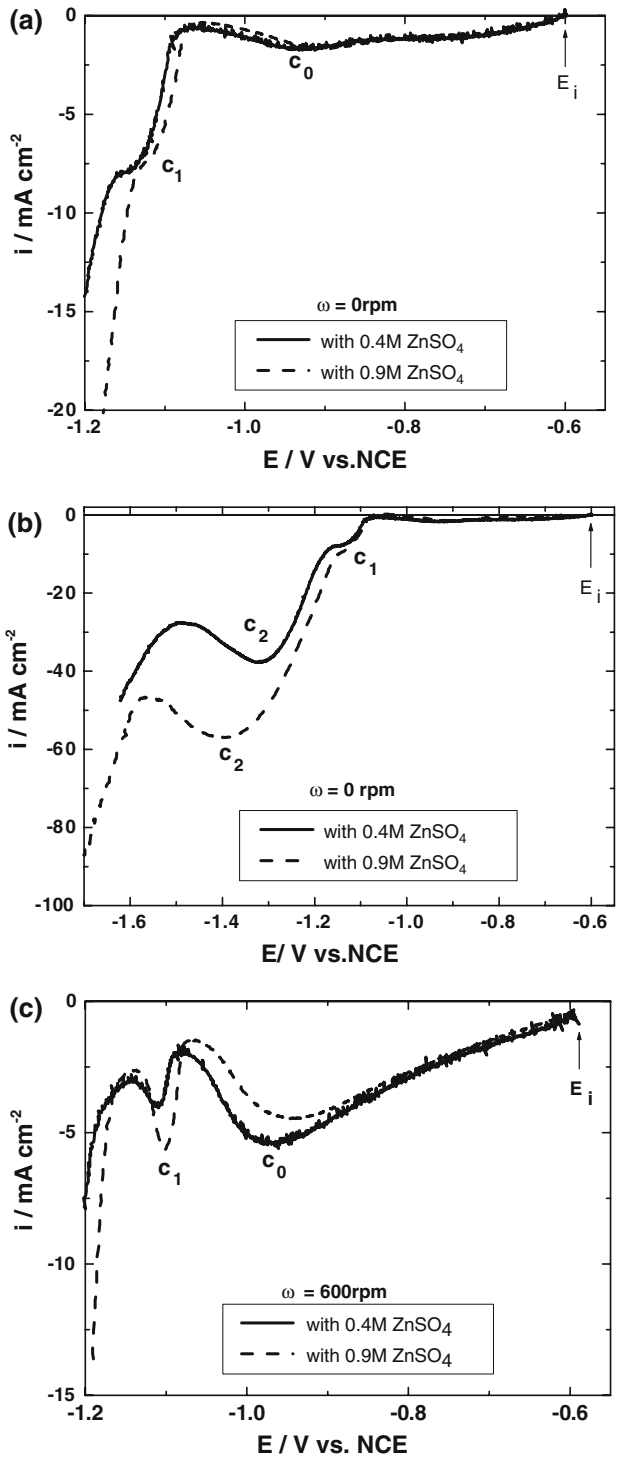

Fig. 6 Typical *i–E* curves for the steel electrode in the zinc electrodeposition solution containing two different concentrations of $ZnSO_4$, as indicated. (**a**) initial behavior; (**b**) complete profile and (**c**) the initial behavior at $\omega = 600$ rpm. For all the cases, $v = 10$ mV s^{-1}. E_i: starting potential

disregarding the pre-bulk deposition region. It can be seen in Fig. 8a, firstly, that H_3BO_3 has a negligible effect on the $|q_a/q_c|$ ratio. Secondly, this ratio decreases with increasing ω, reflecting the lower coverage of the steel surface by Zn under rotating conditions, since the enhanced HER on steel will affect the $|q_a/q_c|$ ratio. Thus, at pH 5, $|q_a/q_c|$ is higher than at pH 2 when $\omega > 0$ (Fig. 8a), as expected. At $\omega = 0$ rpm, the highest $|q_a/q_c|$ ratios are observed, irrespective of pH and also, very close to that for $[Zn^{2+}] = 0.9$ M (see Fig. 8b). In relation to this, despite the higher overpotential attained at E_λ of -1.19 V for the 0.9 M solution, at $\omega = 0$ rpm, there is practically no dependence of $|q_a/q_c|$ on $[Zn^{2+}]$. In Fig. 8b, at $\omega = 600$ rpm, the difference in $|q_a/q_c|$ is very high and, even allowing for the distinct overpotentials, this result again indicates a higher steel surface coverage by Zn at higher $[Zn^{2+}]$.

From the above results, it can be concluded that the Zn electrodeposition on steel from the solution analyzed here initially involves Zn upd together with the HER from H_3O^+ reduction, in the pre-bulk electrodeposition region, followed by bulk electrodeposition involving a primary nucleation and growth of Zn in region c_1, followed by secondary nucleation and growth. All the bulk electrodeposition processes are dependent on the pre-bulk degree of coverage during Zn upd. This explains the atypical behavior of c_1 when stationary and rotating electrode conditions are compared (Fig. 2). Where there is a smaller quantity of Zn upd and lower coverage as in rotating electrode conditions, smaller current densities will be attained in c_1.

It is not clear how the bulk processes depend on the pre-bulk ones, but it seems that the primary nucleation must occur over the Zn upd layer patches. Nucleation and growth on top of previously formed upd layers are known in the literature and described by the Stranski-Krastanov or Frank-van der Merwe mechanisms [61]. The patches of Zn upd act as active sites for Zn growth in the primary nucleation and growth. This means that, on the steel surface uncovered by Zn upd, there is a negligible number of active sites for Zn nucleation in the potential region of c_1. For the stationary electrode, the electrode surface is practically all covered by Zn upd in the pre-bulk electrodeposition region and a much higher number of Zn nuclei are formed, leading to the higher observed current densities than those for rotating electrode conditions.

Additionally, the primary nucleation and growth is diffusion controlled, as can be seen from the dependence of c_1 on ω in Fig. 7. The existence of diffusion control of bulk deposition under forced convection conditions in region c_1 means that the current density must be concentrated on the small number of nuclei formed on the Zn upd layer. This would give rise to individual hemispherical nucleus diffusion zones around each nucleus which can collide with each other (soft collision), generating exclusion zones [62] and hindering nucleation and growth on the included active sites. Under stationary electrode conditions, the Zn upd

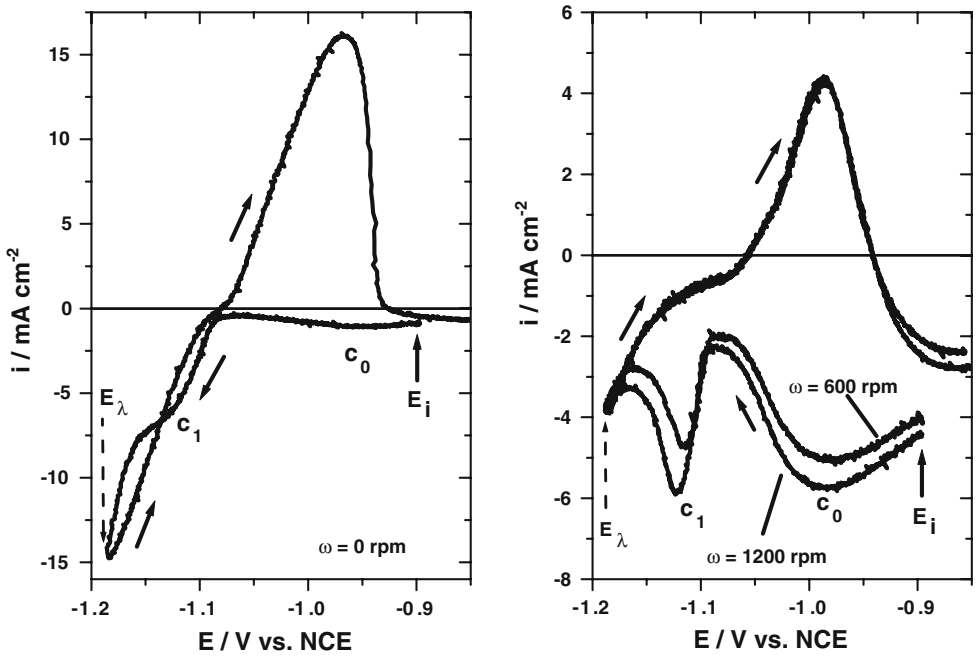

Fig. 7 Typical *i–E* curves for the steel electrode in the zinc electrodeposition solution (0.4 M $ZnSO_4 \cdot 7H_2O$ + 0.3 M H_3BO_3 + 1 M NH_4Cl) at different ω, as indicated, for a switching potential (E_λ) of −1.19 V. $v = 10$ mV s^{-1}

must cover practically the whole electrode surface and a large number of nuclei are thus formed. As a consequence, the current is distributed over almost the entire electrode surface and not concentrated on the small number of nuclei formed under rotating conditions. The diffusion control will thus appear at higher current densities as visualized in the c_1 shoulder in Fig. 2.

The secondary nucleation and growth after c_1 also depends on the previous quantity of Zn electrodeposited. It is much less favored when a small amount of Zn has been electrodeposited within c_1 (rotating electrode). At more negative potentials, Zn electrodeposition will occur at active sites on the steel surface and also on the Zn electrodeposited during the primary nucleation. The exclusion zones around the growing Zn nuclei from the primary nucleation, to some extent hinder the secondary nucleation onset.

3.1.3 The effects of Co^{2+} on the Zn electrodeposition

The effects of Co^{2+} on the cathodic electrochemical curves of Zn electrodeposition can be seen in Fig. 9. There is practically no effect on the pre-bulk electrodeposition region, but, as [Co^{2+}] increases, the current densities attained at the plateau of process c_1 are reduced. Also, the new increase in current density beyond c_1 (towards c_2) is displaced to more negative potentials. It is observed, at least at the beginning, that the ZnCo electrodeposition curves are very similar to those for Zn electrodeposition, maintaining all the characteristics discussed in 3.1.2 for bulk electrodeposition.

The current density of peak c_2 is also gradually diminished with increasing [Co^{2+}] and shifts to more negative potentials. Also, the well-defined peak c_2 produced at 0 M Co^{2+} is gradually converted to a shoulder at the highest [Co^{2+}]. This might be the result of the HER occurring on a deposit rich in Co and/or Co^{2+} reduction itself.

3.2 The electrodeposition of Co and ZnCo

The *i–E* curves for Co^{2+} reduction and the effects on them of adding Zn^{2+} are shown in Fig. 10. Specifically in stationary electrode conditions (Fig. 10a), as expected, the electrodeposition of Co, which is nobler than Zn, starts to occur at more positive potentials than that of Zn. The Co electrodeposition curve in Fig. 10a is characterized firstly by a wave, labelled $c_{Co,1}$, then a peak $c_{Co,2}$ at a potential of approximately −1.15 V and, after that, a new increase in current density is observed, related to the HER on Co together with Co^{2+} reduction. The peak $c_{Co,2}$ has the same maximum current density as that for Zn electrodeposition (curve 2), as expected from their equal molarity (0.4 M). All the processes are mass-transfer controlled.

The *i–E* profiles shown in Fig. 10 for Co electrodeposition suggest that Co^{2+} reduction has two steps. The wave $c_{Co,1}$ is not in the upd region since the Nernst reversible potential for 0.4 M Co^{2+} at 25 °C is approximately −0.57 V. Also, it cannot be related to reduction of a Co^{2+}

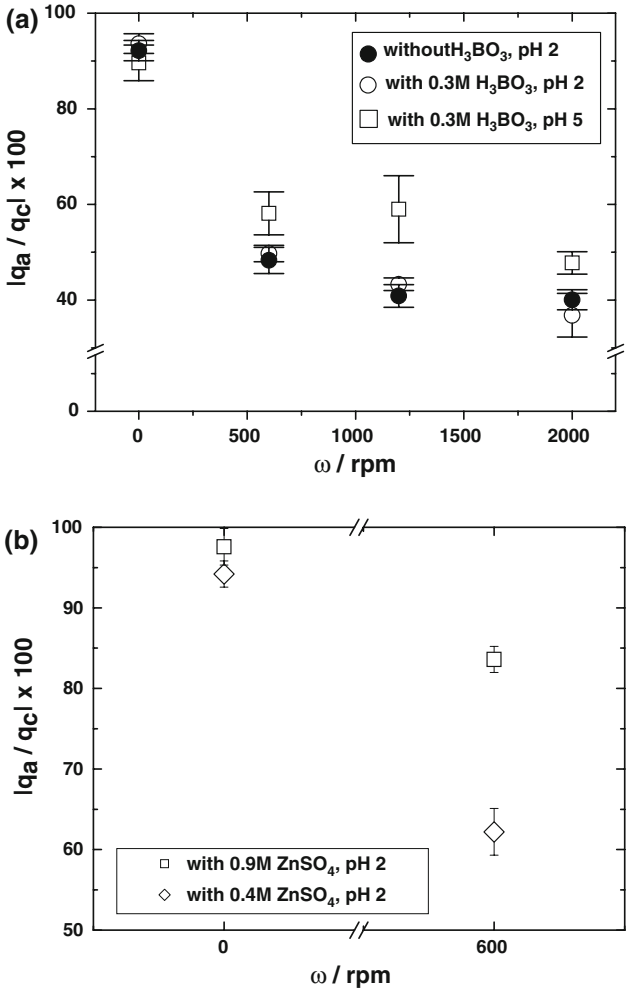

Fig. 8 The dependence of the $|q_a/q_c|$ ratio for voltammetric zinc electrodeposition (**a**) on ω, pH and presence of H_3BO_3, at $[ZnSO_4] = 0.4$ M and (**b**) on $[ZnSO_4]$, as indicated. All the data corresponds to an E_λ of -1.19 V as the ones in Fig. 7

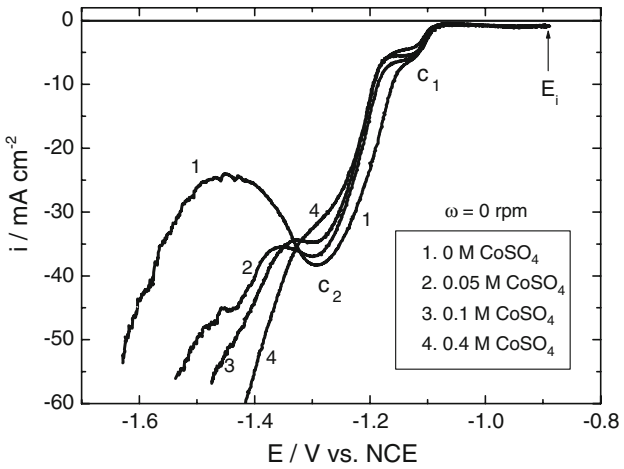

Fig. 9 Typical i–E curves for the steel disk electrode in the Zn electrodeposition solution (0.4 M $ZnSO_4 \cdot 7H_2O$ + 0.3 M H_3BO_3 + 1 M NH_4Cl) under stationary electrode conditions, with various concentrations of $CoSO_4$ added to the solution. $v = 10$ mV s^{-1}. E_i: starting potential

complex with NH_3 since, at pH 2, $Co(H_2O)_6^{2+}$ is the predominant species [63–65]. Direct reduction of Co^{2+} is assumed by Matsushima et al. [66], at pH = 3, and Grujicik and Pesic [64] at pH = 6. Regarding H_3BO_3, it is assumed it has no effect on this behavior since H_3BO_3 is related to changes in the morphology of Co deposits [67–69]. From the work of Kleinert et al. [70], the electrodeposition of Co shown in Fig. 10 can be interpreted as a slow Co^{2+} reduction in parallel with the HER on newly formed Co nuclei at the beginning and, at more negative potentials, as a faster Co^{2+} reduction, giving rise to peak $c_{Co,2}$.

In Fig. 10, if Zn^{2+} is present in the Co electrodeposition solution, the Co^{2+} reduction at the beginning is practically inhibited and the i–E profile is very close to that of pure Zn electrodeposition (Fig. 1). EDX analysis of ZnCo films electrodeposited at various galvanostatic current densities (i_g) is shown in Fig. 11 as the variation of [Co/Zn] ratio with i_g. The Co content in these ZnCo deposits was very low, varying between 0.3 and 0.6 wt.%. However, this composition is a useful one for the purpose of corrosion protection [33].

The data in Fig. 10 show that, before c_1, Zn^{2+} hinders the HER considerably but it also hinders Co^{2+} reduction. This is a well-known effect in ZnCo electrodeposition [37, 39–42, 71], even with a much lower $[Zn^{2+}]$ than $[Co^{2+}]$ [39, 41]. Some authors consider that Co^{2+} assists Zn^{2+} reduction and that the hindering of Co electrodeposition appears only above a certain percentage of Zn in the deposit [43, 44]. Before this hindering of Co^{2+} reduction by Zn^{2+} occurs, there must be some Co electrodeposited on the steel. This Co can act as a center for Zn^{2+} adsorption and this is also postulated as one reason for the subsequent hindering of Co^{2+} reduction [37, 38]. It is expected that at high $[Co^{2+}]$, larger quantities of Co will be electrodeposited before Co^{2+} reduction starts to be hindered by Zn^{2+} reduction.

The ZnCo electrodeposition curves under forced convection being very similar to those of Zn, the pre-bulk upd layer and the primary and secondary nucleation and growth processes must also be present.

4 Conclusions

Zinc electrodeposition onto steel from acid sulfate solutions exhibits a pre-bulk electrodeposition region where Zn upd competes with the parallel hydrogen evolution reaction from H_3O^+ reduction (HER). Under forced convection conditions, the HER is faster and only small quantities of Zn upd are formed.

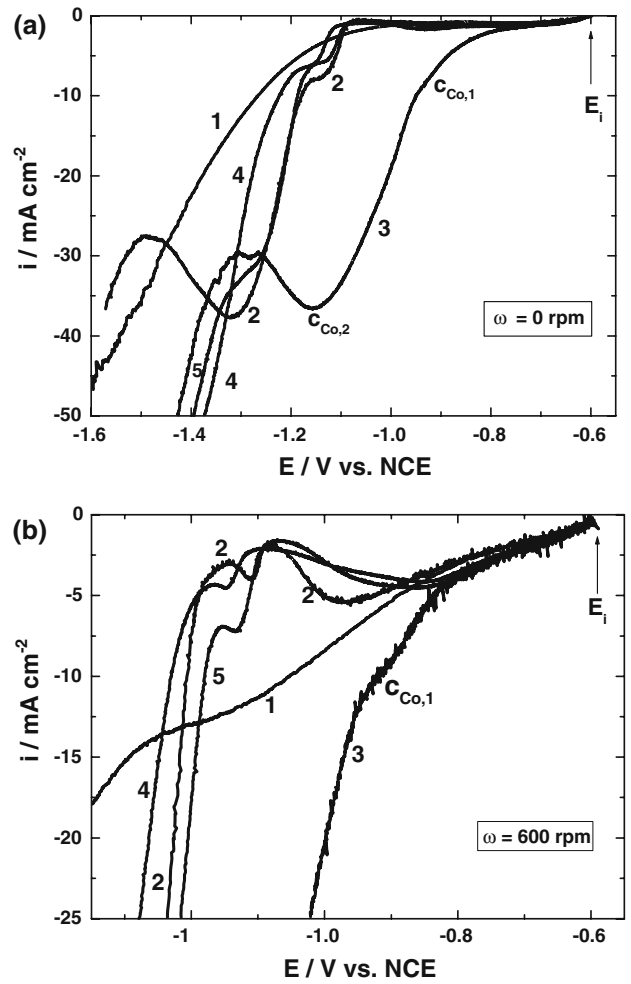

Fig. 10 Typical *i–E* curves for the steel electrode in : (1) blank solution (0.3 M H_3BO_3 + 1 M NH_4Cl); (2) Zn electrodeposition solution (0.4 M $ZnSO_4$ + 0.3 M H_3BO_3 + 1 M NH_4Cl); (3) Co electrodeposition solution (0.4 M $CoSO_4$ + 0.3 M H_3BO_3 + 1 M NH_4Cl); (4) ZnCo electrodeposition solution (0.4 M $CoSO_4$ + 0.1 M $ZnSO_4$ + 0.3 M H_3BO_3 + 1 M NH_4Cl); (5) ZnCo electrodeposition solution (0.4 M $CoSO_4$ + 0.4 M $ZnSO_4$ + 0.3 M H_3BO_3 + 1 M NH_4Cl). (**a**) Stationary and (**b**) rotating electrode conditions. $v = 10$ mV s^{-1}. E_i: starting potential

The bulk electrodeposition of Zn is initiated with primary nucleation and diffusion-controlled growth, followed by secondary nucleation and growth. Primary nucleation and growth seems to occur on top of the previously formed Zn upd layer. Smaller surface coverage of the electrode by bulk electrodeposited Zn occurs under forced convection conditions, where Zn upd is also small, due to high HER.

The electrodeposition of Co on steel is strongly hindered by Zn^{2+} in solution.

The ZnCo electrodeposition curves are very similar to those of Zn^{2+} reduction, especially at the beginning, even with equal concentrations of Zn^{2+} and Co^{2+} in solution. They also exhibit a pre-bulk electrodeposition region followed by primary and secondary nucleation and growth.

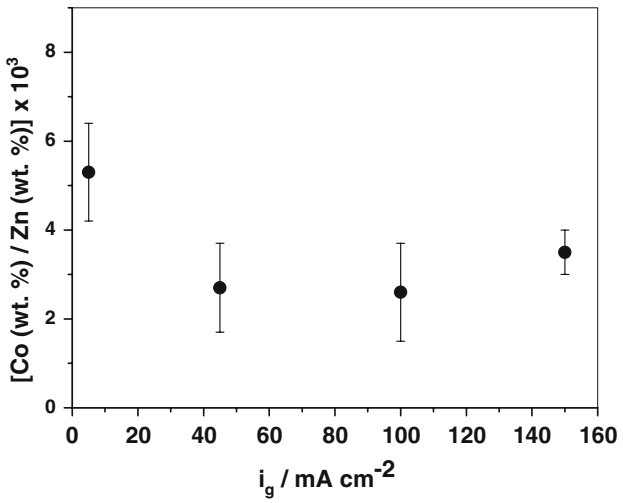

Fig. 11 Variation of [Co (wt.%)/Zn (wt.%)] ratio in 80 C cm^{-2} ZnCo films electrodeposited at $\omega = 600$ rpm, as a function of i_g

Acknowledgements P. C. Tulio is grateful to Fundação de Amparo à Pesquisa do Estado de São Paulo (FAPESP) for his Ph. D. grant.

References

1. Musiani M (2000) Electrochim Acta 45:3397
2. Hovestad A, Janssen LJJ (1995) J Appl Electrochem 25:519
3. Oberle RR, Scanlon MR, Cammarata RC et al (1995) Appl Phys Lett 66:19
4. Verelst M, Bonino JP, Rousset A (1991) Mater Sci Engineer A 315:51
5. Wu G, Li N, Zhou D et al (2004) Surf Coat Technol 176:157
6. Pavlatou EA, Stroumbouli M, Gyftou P et al (2006) J Appl Electrochem 36:385
7. Shrestha NK, Sakurada K, Masuko M et al (2001) Surf Coat Technol 140:175
8. Yeh SH, Wan CC (1995) Mater Sci Technol 11:589
9. Hashimoto S, Abe M (1994) Corr Sci 36:2125
10. Benea L, Bonora PL, Wenger F et al (2002) Proceedings of the 15th Intern Corrosion Congress, Granada, Spain, 22–27 Sept 2002
11. Celis JP, Roos JR, Buelens C (1987) J Electrochem Soc 134:1402
12. Guglielmi N (1972) J Electrochem Soc 119:1009
13. Fransaer J, Celis JP, Roos JR (1992) J Electrochem Soc 139:413
14. Hwang BJ, Hwang CS (1993) J Electrochem Soc 140:979
15. Vereecken PM, Shao I, Searson PC (2000) J Electrochem Soc 147:2572
16. Bozzini B, Brevaglieri B, Cavallotti PL et al (2000) Electrochim Acta 45:3431
17. Benea L, Bonora PL, Borello A et al (2001) J Electrochem Soc 148:C461
18. Watson SW (1993) J Electrochem Soc 140:2235
19. Socha RP, Nowak P, Laajalehto K et al (2004) Colloids Surf A 235:45
20. Lee EC, Choi JW (2001) Surf Coat Technol 148:234
21. Nowak P, Socha RP, Kaisheva M et al (2000) J Appl Electrochem 30:429
22. Webb PL, Robertson NL (1994) J Electrochem Soc 141:669
23. Zhang XG (1996) Corrosion and electrochemistry of zinc. Plenum Press, New York
24. Lowenheim F (1974) Modern electroplating. Wiley, New York

25. Gomes A, da Silva Pereira MI (2006) Electrochim Acta 52:863
26. Gomes A, da Silva Pereira MI (2006) Electrochim Acta 51:1342
27. Méndez PF, López JR, Meas Y et al (2005) Electrochim Acta 50:2815
28. Díaz-Arista P, Meas Y, Ortega R et al (2005) J Appl Electrochem 35:217
29. Tripathy BC, Das SC, Singh P et al (2004) J Electroanal Chem 565:49
30. Kim J, Lee J, Park S (2004) Langmuir 20:459
31. Lee JY, Kim JW, Lee MK et al (2004) J Electrochem Soc 151:C25
32. Alvarez AE, Salinas DR (2004) J Electroanal Chem 566:393
33. Wilcox GD, Gabe DR (1993) Corr Sci 35:1251
34. Nicol MJ, Philip HI (1976) J Electroanal Chem 70:233
35. Higashi K, Fukushima H, Urakawa T et al (1981) J Electrochem Soc 128:2081
36. Fabri Miranda FJ, Barcia OE, Mattos OR et al (1997) J Electrochem Soc 144:3441
37. Gómez E, Alcobe X, Vallés E (2001) J Electroanal Chem 505:54
38. Gómez E, Vallés E (1997) J Electroanal Chem 421:157
39. Alcalá ML, Gómez E, Vallés E (1994) J Electroanal Chem 370:73
40. Karwas C, Hepel T (1989) J Electrochem Soc 136:1672
41. Yunus M, Capel-Boute C, Decroly C (1965) Electrochim Acta 10:885
42. Mindowickz J, Capel-Boute C, Decroly C (1965) Electrochim Acta 10:901
43. Fratesi R, Roventi G, Giuliani G et al (1997) J Appl Electrochem 27:1088
44. Roventi G, Fratesi R, Della Guardia RA et al (2000) J Appl Electrochem 30:173
45. Takahashi A, Miyoshi Y, Hada T (1994) J Electrochem Soc 141:954
46. Tulio PC, Rodrigues SEB, Carlos IA (2007) Surf Coat Technol 202:91
47. D′Alkaine CV, Tulio PC, Mahmud Z (2000) Proceedings X Brazilian Meeting and Exposition on Surface Treatments (X EBRATS), São Paulo, Brazil
48. Zech N, Landolt D (2000) Electrochim Acta 45:3461
49. Despic AR, Pavlovic MG (1982) Electrochim Acta 27:1539
50. Casanova T, Soto F, Eyraud M et al (1997) Corr Sci 39:529
51. Zheng G, Popov BN, White RE (1995) J Appl Electrochem 25:212
52. Rashkov S, Bozhkov C, Kudryavtsev V et al (1988) J Electroanal Chem 248:421
53. Raeissi K, Saatchi A, Golozar MA et al (2005) Surf Coat Technol 197:229
54. Maja M, Penazzi N, Fratesi R et al (1982) J Electrochem Soc 129:2695
55. Raeissi K, Saatchi A, Golozar MAJ (2003) Appl Electrochem 33:635
56. Baugh LM (1979) Electrochim Acta 24:657
57. Baugh LM (1979) Electrochim Acta 24:669
58. Cachet C, Wiart R (1990) J Appl Electrochem 20:1009
59. Park JR, Kim HT (1999) Plat Surf Finish 86:108
60. Rashkov S, Petrova M, Bozhkov C (1990) J Appl Electrochem 20:11
61. Budevski E, Staikov G, Lorenz WJ (1996) Electrochemical phase formation and growth. VCH, New York
62. Fletcher S (1981) J Electroanal Chem 118:419
63. Soto AB, Arce EM, Palomar-Pardavé M et al (1996) Electrochim Acta 41:2647
64. Grujicik D, Pesic B (2004) Electrochim Acta 49:4719
65. Palomar-Pardavé M, González I, Soto AB et al (1998) J Electroanal Chem 443:125
66. Matsushima JT, Trivinho-Strixino F, Pereira EC (2006) Electrochim Acta 51:1960
67. Jeffrey MI, Choo WL, Breuer PL (2000) Min Engineer 13:1231
68. Cavallotti PL, Vicenzo A, Bertetti M et al (2003) Surf Coat Technol 169–170:76
69. Vicenzo A, Cavallotti PL (2004) Electrochim Acta 49:4079
70. Kleinert M, Waibel H-F, Engelmann GE et al (2001) Electrochim Acta 46:3129
71. Rashwan SM, Mohamed AE, Abdel-Wahaab SM et al (2003) J Appl Electrochem 33:1035